31GHz Ge *n-i-p* waveguide photodetectors on Silicon-on-Insulator substrate

Tao Yin[1*], Rami Cohen[2], Mike M. Morse[1], Gadi Sarid[2], Yoel Chetrit[2], Doron Rubin[2], and Mario J. Paniccia[1]

[1]*Intel Corporation, 2200 Mission College Blvd., Santa Clara, CA, 95054, USA*
[2] *Intel Corporation, S.B.I Park Har Hotzvim, Jerusalem, 91031, Israel*
[*]*Corresponding author: tao.yin@intel.com*

Abstract: We report on evanescently coupled Ge waveguide photodetectors that are grown on top of Si rib waveguides. A Ge waveguide detector with a width of 7.4μm and length of 50 μm demonstrated an optical bandwidth of 31.3 GHz at -2V for 1550nm. In addition, a responsivity of 0.89 A/W at 1550 nm and dark current of 169 nA were measured from this detector at -2V. A higher responsivity of 1.16 A/W was also measured from a longer Ge waveguide detector (4.4 x 100 μm^2), with a corresponding bandwidth of 29.4 GHz at -2V. An open eye diagram at 40 Gb/s is also shown.

OCIS codes: (040.5160) Photodetectors; (130.3120) Integrated optics devices; (130.0250) Optoelectronics; (130.1750) Components; (200.4650) Optical interconnects

References and Links

1. A. Liu, L. Liao, D. Rubin, H. Nguyen, B. Ciftcioglu, Y. Chetrit, N. Izhaky, and M. Paniccia, "High-speed optical modulation based on carrier depletion in a silicon waveguide," Opt. Express **15**, 660-668 (2007)
2. Q. Xu, B. Schmidt, S. Pradhan, and M. Lipson, "Micrometre-scale silicon electro-optic modulator," Nature **435**, 325-327 (2005).
3. H. Rong, Richard Jones, Ansheng Liu, Oded Cohen, Dani Hak, Alexander Fang and Mario Paniccia, "A continuous-wave Raman silicon laser," Nature **433**, 725-728 (2005).
4. A. Fang, H. Park, O. Cohen, R. Jones, M, Paniccia and J. Bower, "Electrically pumped hybrid AlGaInAs-silicon evanescent laser," Opt. Express, **14**, 9203-9210 (2006).
5. G. Dehlinger and S. J. Koester and J. D. Schaub and J. O. Chu and Q. C. Ouyang and A. Grill, "High-Speed Germanium-on-SOI Lateral PIN photodiodes," IEEE Photon. Technol. Lett. **16**, 2547-2549 (2004).
6. M. Morse, O. Dosunmu, G. Sarid, and Y. Chetrit, "Performance of Ge-on-Si p-i-n photodetectors for standard receiver modules," IEEE Photon. Technol. Lett. **18**, 2442-2444 (2006).
7. D. Ahn, C. Hong, J. Liu, W. Giziewicz, M. Beals, L.C. Kimerling and J. Michel, "High performance, waveguide integrated Ge photodetectors," Opt. Express **15**, 3916-3921 (2007).
8. L. Vivien, M. Rouviere, J. Fedeli, D. Marris-Morini, J. Damlencourt, J. Mangeney, P. Crozat, L. El Melhaoui, E. Cassan, X. Le Roux, D. Pascal and S. Laval, "High speed and high responsivity germanium photodetector integrated in a Silicon-On-Insulator microwaveguide," Opt. Express **15**, 9843-9848 (2007).
9. C. Gunn, G. Masini, J. Witzens and G. Capellini, "CMOS Photonics Using Germanium Photodetectors," SiGe and Ge: Materials, Processing and Devices, ECS Transcations **3**, 17-24 (2006).
10. H. Luan, K. Wada, L. C. Kimerling, G. Masini, L. Colace, and G. Assanto, "High efficiency photodetectors based on high quality epitaxial germanium grown on silicon substrates," Opt. Mater. **17**, 71-73 (2001).
11. G. Reed and A. Knights, *Silicon Photonics*, (Wiley, 93-97, 2004).
12. I. Day, I. Evans, A. Knigha, F. Hopper, S. Roberts, J. Johnston, **S.** Day, I. Luff, H. Tsang, and M. Asghari, "Tapered Silicon Waveguides for Low Insertion Loss Highly-Efficient High-speed Electronic Variable Optical Attenuators," Optical Fiber Communications Conference, **1**, 249-251 (2003).
13. J. Liu, D. D. Cannon, K. Wada, Y. Ishikawa, S. Jongthammanurak, D. Danielson, J. Michel, and L. C. Kimerling, "Tensile strained Ge *p-i-n* photodetectors on Si platform for C and L band telecommunications," Appl. Phys. Lett. **87**, 011110-1-3 (2005)

1. Introduction

As the aggregate data rate for several applications is approaching or exceeding 100 Gb/s, it is increasingly desirable to develop integrated optical components with reduced size, complexity, and cost. Silicon is one of the candidates on which to integrate, although it

#86625 - $15.00 USD Received 17 Aug 2007; revised 2 Oct 2007; accepted 5 Oct 2007; published 9 Oct 2007

suffers from less than ideal optical properties such as poor light emission efficiency due to an indirect bandgap. Nevertheless, there has been steady progress on several of the required components, including modulators [1, 2], light emitters [3, 4], and detectors [5, 6]. Most of the current research [7-9] on the latter devices is focused on using germanium as the absorbing material. This is due to the much higher absorption coefficient of Ge as compared to Si in the near infrared, as well as its compatibility with standard CMOS processing. The drawback in using pure germanium is the introduction of dislocations which relieve the stress caused by the 4% lattice mismatch between Ge and Si. These defects can lead to increased dark current which can degrade receiver sensitivity and reliability if the processing is not carefully handled [10]. Even with the addition of pure Ge, however, the absorption coefficient at 1550nm is not large enough to support the high speed and high quantum efficiencies needed for surface normal photodetectors typically used in current communication links. The most obvious way around this problem is to use a waveguide-based detector which breaks the trade-off between bandwidth and responsivity present in surface normal detectors, and is much easier to integrate with other types of devices. By increasing the detector length, the responsivity of Ge waveguide detectors can be greatly increased at 1550nm even though the material absorption coefficient is small at this wavelength. The detector speed can also be simultaneously optimized by using a thin Ge layer to reduce transit time limitations. The overall reduction in area and capacitance in going from a normal incident to a waveguide-based photodetector helps to improve receiver sensitivity and enable greater than 20 GHz operation which will be critical in the increasingly important applications of short distance communications.

In this paper, we demonstrate Ge waveguide photodetectors with low dark current, high quantum efficiency and high speed data transmission capability that will enable them to be readily used in both next generation communication networks and optical interconnects in future computing applications.

2. Device structure and fabrication

The layout of the waveguide photodetector and schematic cross-section are shown in Figs. 1(a) and 1(b), respectively. As the light propagates from the rib waveguide to the photodetector region, the light evanescently couples up into the overlying Ge region where absorption occurs. The processing was done on 100 Ω-cm SOI wafers with a 1 μm thick buried oxide and a Si thickness of 1.5 μm. Before the waveguides were patterned, the substrate was locally implanted with boron only in the regions where the detectors would be fabricated to minimize both free carrier loss and parasitic capacitance between the substrate and contact metal pads. The Si rib waveguides were then formed by etching the substrate 0.6 μm deep, with a width of 1.4 μm. Lateral tapers, etched in the same step, were used to improve the coupling between the fiber and single-mode Si waveguide, as well as between the Si waveguide and the wider Ge waveguide photodetector. The width of the taper at the input was 4.5 μm. After oxide deposition and patterning, a 1.3 μm thick film of Ge was grown by a selective epitaxial process. The growth consisted of a 0.1μm thick low temperature Ge buffer layer followed by 1.2 μm of Ge grown at 700°C. The Ge film was intentionally grown thicker than the final target thickness so that we could planarize the Ge with a chemical-mechanical polishing (CMP) step. A final Ge thickness of 0.8μm was obtained after CMP, a thickness which is optimized by modeling for both evanescent coupling at 1550 nm into the Ge and high bandwidth operation. These wafers then underwent a Ge anneal to reduce the threading dislocation density. Phosphorous was implanted into the top of the Ge film to form a vertical *n-i-p* junction, with the boron-implanted Si substrate serving as the anode. Another localized boron implant was also done into the Si to improve the ohmic contact between the metal contacts and implanted Si substrate. Dopant activation was done by rapid thermal annealing (RTA) at 650°C for 10 seconds. Finally, 1 μm of Al was deposited and patterned to form the metal contacts of the detector. . A SEM cross-section of the completed device is shown in Fig. 1(c).

#86625 - $15.00 USD Received 17 Aug 2007; revised 2 Oct 2007; accepted 5 Oct 2007; published 9 Oct 2007

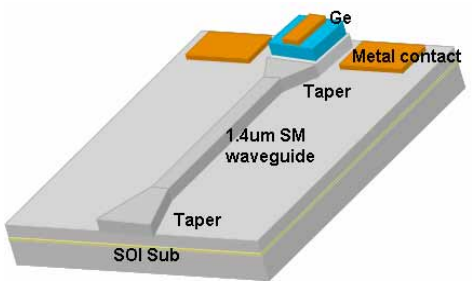

(a)

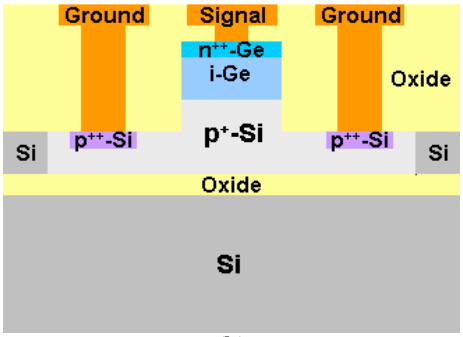

(b)

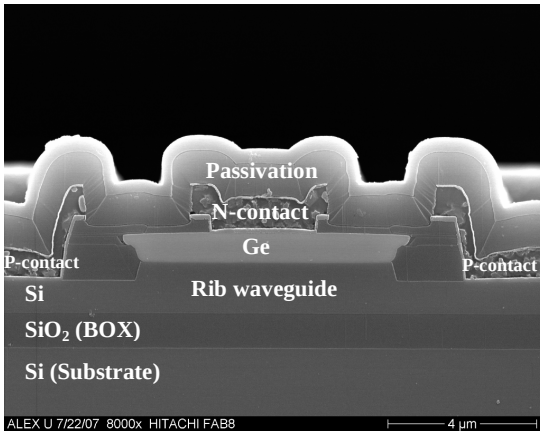

(c)

Fig. 1. (a). Schematic layout for the Ge detector integrated with a passive waveguide. (b) Cross-section schematic of the Ge ***n-i-p*** waveguide photodetector. (c) Cross-section SEM image of the Ge waveguide photodetector (7.4µm x 50µm) after processing.

3. Results and discussions

Results from two waveguide photodetector dimensions are presented here; detector A has a width of 7.4µm and a length of 50µm, while detector B is 4.4µm x 100µm. Figure 2(a) shows the measured photocurrent and dark current within a voltage range of -5V to 0.6V for both devices. The dark current at -2V was measured at 169nA and 267nA for detectors A and B, respectively, corresponding to dark current densities of 51mA/cm^2 and 74mA/cm^2 based on

#86625 - $15.00 USD Received 17 Aug 2007; revised 2 Oct 2007; accepted 5 Oct 2007; published 9 Oct 2007

the effective active area of the devices. Contributions to the dark current can come from the bulk and sidewalls, so both need to be dealt with to get the lowest possible value. While the growth and annealing conditions were used to reduce the former component, passivation and implantation location were used for the latter. Specifically, the edge of the phosphorous implantation in the Ge film was intentionally pulled in from the Ge sidewalls by 0.4um on each side to minimize the E-field at these trap-laden interfaces, thereby reducing the level of surface leakage current.

The photocurrent was measured using a lensed fiber with a 2μm spot size to couple light into a 4.5μm wide lateral taper. In order to calculate the responsivity of the Ge photodetector, the coupling loss and transmission loss of the silicon rib waveguide were characterized through measurement on rib waveguides without Ge detectors. By using the Fabry-Perot (FP) method [11], the measured average transmission loss of the Si rib waveguide, together with input taper and reverse taper, was calculated to be -0.55 ±0.05 dB/cm at 1550nm. The average coupling loss at the input facet was measured to be -3.0dB ±0.3dB. By using a vertical taper to match the incoming fiber mode, the coupling loss can be reduced to less than -1dB [12]. A negligible difference in transmission loss was observed between the 4.4μm and 7.4μm wide waveguides because of the fundamental mode excitation for both waveguides by using the taper structures. Taking into consideration the input facet coupling loss and the Si waveguide transmission loss before reaching Ge waveguide detector, the power reaching the Ge detector was calculated to be ~126μW. Therefore, the responsivities for detectors A and B were calculated to be 0.89A/W ±0.06A/W and 1.16A/W ±0.08A/W at -2V, respectively, corresponding to quantum efficiencies of 71% and 93% at 1550nm. Beamprop modeling revealed a local maxima in absorption at 1550 nm in the Ge region when the Ge thickness was 0.8μm, where the absorption coefficient of 4000cm^{-1} for tensile strained Ge was used [13]. The free carrier loss caused by the heavy doping of $1x10^{18}cm^{-3}$ for rib waveguide underneath the 100μm long detector region is calculated to be -0.1dB. In addition, the scattering loss from rib waveguide region to Ge/Si region accounts for 2%-5% losses based on the measurement because the majority of mode is confined in the rib waveguide.

Ge waveguide detectors with a width of 4.4μm and length of 250μm exhibit no further increase in photocurrent compared to their 100μm long counterparts, indicating that virtually all the light was absorbed within the first 100 μm of Ge. The detector length for reaching total absorption is subject to both the material absorption coefficient and mode coupling from the Si rib waveguide to the Ge active region. Coupling to the Ge layer can be improved by optimizing Ge layer thickness and reducing the rib waveguide height, allowing for even shorter detectors. However the trade-off for reducing the rib height is increased polarization sensitivity, which would reduce the viability of such waveguide detectors. For the detectors discussed in this paper, the measured polarization dependence is smaller than 1dB.

Figure 2 (b) shows the measured responsivity over a wavelength range of 1500 nm to 1618 nm for detectors A and B at -2V. A flat responsivity was measured for wavelengths out to 1560-1570nm, beyond the absorption edge of bulk Ge due to the tensile-strain induced bandgap narrowing [13]. The responsivity at 1610nm was measured at 0.34A/W and 0.41A/W at -2V for detectors A and B, respectively.

#86625 - $15.00 USD Received 17 Aug 2007; revised 2 Oct 2007; accepted 5 Oct 2007; published 9 Oct 2007

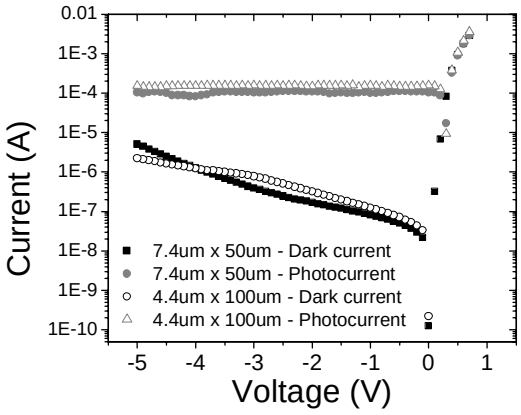

(a)

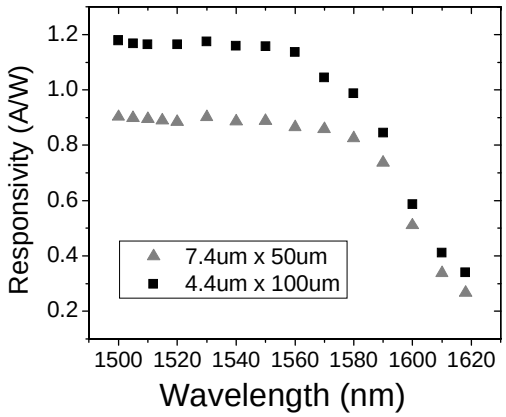

(b)

Fig. 2. (a). Measured dark current and photocurrent with input optical power of 126μW at 1550nm for detector 7.4μm x 50μm and 4.4μm x 100μm. (b) Responsivity versus wavelength for detector 7.4μm x 50μm, and detector 4.4μm x 100μm, respectively, at -2V.

The frequency response of these detectors was measured by using a lightwave component analyzer that provides measurement capability out to 67GHz. A modulated optical signal at 1550nm with an average power of 278μW was launched into the waveguide detector and the electrical output was measured through a high speed RF probe. The frequency response of the bias-tee, RF cables, and probe were factored out from the result. Figure 3 shows the normalized optical response for detectors A and B at -2V, and the inset shows the optical bandwidth versus voltage for the two detectors. The optical bandwidths of detectors A and B was measured to be 31.3GHz and 29.4GHz, respectively, at -2V. The corresponding electrical (power) bandwidths are 26GHz and 24.1GHz. At 0V bias, detectors A and B still achieve optical bandwidths of 15.7GHz and 10GHz, respectively. It can be seen that the bandwidths decrease with increasing device area due to increased RC delay. With the intrinsic Ge thickness of 0.7μm (total Ge thickness 0.8μm), the calculated depletion capacitance is 66.7fF and 72.8fF for detectors A and B. The pad capacitance is measured to be 23fF. Modeling suggested that optimum bandwidth is achieved at this Ge thickness for both detectors, and that

#86625 - $15.00 USD Received 17 Aug 2007; revised 2 Oct 2007; accepted 5 Oct 2007; published 9 Oct 2007

the bandwidth is limited by both transit time and RC delay. The predicted electrical bandwidths for detectors A and B were 27 and 26 GHz, respectively, which are consistent with the measured results.

An impulse measurement at 1550nm was also carried out and the converted frequency response from Fast Fourier Transform (FFT) shows that the optical 3-dB bandwidth of detector A is 31GHz, in agreement with the frequency domain measurement.

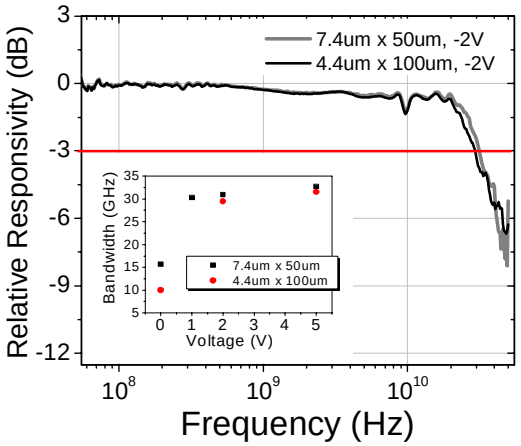

Fig. 3. Measured frequency response for detector 4.4μm x 100μm and 7.4μm x 50μm at -2V, and the inset shows optical bandwidth versus supply voltage for both detectors.

To gauge the viability of using these Ge waveguide detectors in a 40Gb/s system, 40Gb/s data transmission was measured using a Digital Communication Analyzer (DCA) with a 63GHz electrical module. The RF signal from a pseudo-random bit sequence (PRBS) generator with $[2^{31}-1]$ pattern length was used to modulate 1550nm light through a commercially available 40Gb/s $LiNbO_3$ modulator, and the modulated optical signal was fiber coupled to the Ge waveguide detector. A 50GHz RF probe was used to measure the detector output. An RF power amplifier with 16dB gain was used to amplify the detector output for the DCA measurement. Despite the fact that there was no impedance matching between the detector and amplifier, we were able to obtain open eye diagrams from detectors A and B at 40Gb/s, as shown in Fig. 4. The issues in this setup which limited the eye measurement include electrical reflections due to impedance mismatch, as can be seen from the double traces on the rising and falling edges. A very high average power of 1.2mW also had to be launched into the detector due to the limited gain from the RF amplifier, and this could have lead to carrier screening and a slightly slower response time. By properly packaging the Ge waveguide photodetector with a high speed trans-impedance amplifier (TIA) with impedance matching, we expect the high speed data transmission at 40Gb/s to be further improved.

#86625 - $15.00 USD Received 17 Aug 2007; revised 2 Oct 2007; accepted 5 Oct 2007; published 9 Oct 2007

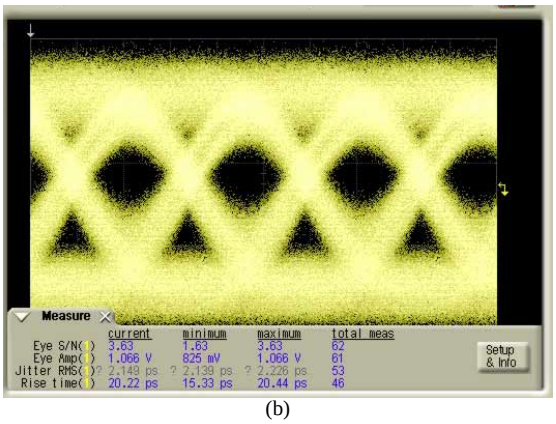

(b)

Fig. 4. Measured eye diagram at 40Gb/s for detector 7.4μm x 50μm at -5V.

4. Summary

We report evanescently coupled Ge waveguide photodetectors that have achieved an optical bandwidth of 29.4 GHz with 93% quantum efficiency at 1550 nm, and 267 nA of dark current at 2V bias. To the best of our knowledge, this bandwidth-efficiency product of 27.3 GHz is the highest reported for any Ge photodetector at 1550 nm. A different size waveguide detector had a slightly higher bandwidth of 31.3 GHz with a reduced quantum efficiency of 71% and a dark current of 169 nA. The dark current and operating voltage are also compatible with typical TIA specifications, making them good candidates for high data rate applications, including 40 Gb/s operation.

Acknowledgment

The authors wish to thank Olufemi Dosunmu and Yimin Kang for fruitful discussions and Ansheng Liu for early simulation support. They also appreciate the support on testing and characterization from Ling Liao, Juthika Basak, Richard Jones, Miriam Reshotko from Intel Corporation as well as David Jackson and Stephen Didde from Agilent Technologies.

#86625 - $15.00 USD Received 17 Aug 2007; revised 2 Oct 2007; accepted 5 Oct 2007; published 9 Oct 2007